# Electrohydrodynamic thrust for in-atmosphere propulsion

Nicolas Monrolin, Franck Plouraboué, Olivier Praud

▶ **To cite this version:**

Nicolas Monrolin, Franck Plouraboué, Olivier Praud. Electrohydrodynamic thrust for in-atmosphere propulsion. AIAA Journal, 2017, vol. 55 (n° 12), pp. 4296-4305. 10.2514/1.J055928 . hal-01660600

**HAL Id: hal-01660600**
**https://hal.science/hal-01660600**

Submitted on 11 Dec 2017

**HAL** is a multi-disciplinary open access archive for the deposit and dissemination of scientific research documents, whether they are published or not. The documents may come from teaching and research institutions in France or abroad, or from public or private research centers.

L'archive ouverte pluridisciplinaire **HAL**, est destinée au dépôt et à la diffusion de documents scientifiques de niveau recherche, publiés ou non, émanant des établissements d'enseignement et de recherche français ou étrangers, des laboratoires publics ou privés.


Open Archive TOULOUSE Archive Ouverte (OATAO)
OATAO is an open access repository that collects the work of Toulouse researchers and makes it freely available over the web where possible.

This is an author-deposited version published in : http://oatao.univ-toulouse.fr/
Eprints ID : 18415

**To link to this article** : DOI: 10.2514/1.J055928
URL : http://dx.doi.org/10.2514/1.J055928

**To cite this version** : Monrolin, Nicolas and Plouraboué, Franck and Praud, Olivier *Electrohydrodynamic thrust for in-atmosphere propulsion.* (2017) AIAA Journal. pp. 1-10. ISSN 0001-1452

Any correspondence concerning this service should be sent to the repository administrator: staff-oatao@listes-diff.inp-toulouse.fr

# Electrohydrodynamic Thrust for In-Atmosphere Propulsion

N. Monrolin,* F. Plouraboué,† and O. Praud‡
*Institut de Mécanique des Fluides de Toulouse (IMFT), Université de Toulouse, CNRS-INPT-UPS, 31400 Toulouse, France*

DOI: 10.2514/1.J055928

**The electrohydrodynamic thrust generated by wire–cylinder electrodes under high dc voltage is experimentally analyzed. Some recent experimental studies have shown that electrohydrodynamic thrusters produced by corona discharge and ionic wind are able to deliver high thrust-to-power ratio, which reopens prospects for electrohydrodynamic propulsion. From simple considerations based on ultralight aircraft mass, aerodynamics, battery mass, and experimental electrohydrodynamic thrust densities, their potential for applications is showcased. Furthermore, an experimental study is performed, for which the experimental observations are presented in terms of electric field and thrust density. This allows a simplified and synthetic presentation of propulsive properties. Various experimental biases have been identified and corrected. The measure of time-periodic oscillations of the airflow in the back of the thruster pinpoints a possible wake effect due to the impact of ionic wind on electrodes. The variations of the associated drag are studied when varying the position of the collecting electrodes. It is shown that aerodynamic losses can be significant in experimental electrohydrodynamic thrusters.**

## Nomenclature

| | | |
|---|---|---|
| $C$ | = | dimensional corona current parameter, $A \cdot V^{-2}$ |
| $C_0$ | = | nondimensional corona current parameter |
| $D$ | = | net drag, N |
| $d$ | = | distance between electrodes, m |
| $d_{\text{drift}}$ | = | effective drift distance of the ions, m |
| $\boldsymbol{E}$ | = | electric field, $V \cdot m^{-1}$ |
| $E^*$ | = | energetic density of batteries, $W \cdot h \cdot kg^{-1}$ |
| $\bar{e}$ | = | time-averaged hot-wire probe signal, |
| $e'$ | = | hot-wire probe signal fluctuations, |
| $F_{\text{EHD}}$ | = | net electrohydrodynamic forces, N |
| $f$ | = | frequency, Hz |
| $\boldsymbol{f}$ | = | volumetric force, $N \cdot m^{-3}$ |
| $g$ | = | gravity acceleration, $m \cdot s^{-2}$ |
| $I$ | = | net electric current, A |
| $i$ | = | electric current per unit length, $A \cdot m^{-1}$ |
| $\boldsymbol{j}$ | = | current density, $A \cdot m^{-2}$ |
| $L/D$ | = | lift-to-drag ratio or glide ratio, |
| $l$ | = | length of the electrodes, m |
| $M$ | = | net mass of the airplane, kg |
| $m_a$ | = | mass without battery, kg |
| $m_b$ | = | mass of embedded battery, kg |
| $P_e$ | = | electric power input, W |
| $Re$ | = | Reynolds number |
| $r_c$ | = | collector radius, m |
| $r_e$ | = | emitter radius, m |
| $S_w$ | = | wetted surface, $m^2$ |
| $St$ | = | Strouhal number |
| $s$ | = | spacing between collecting electrodes, m |
| $T$ | = | net Thrust, N |
| $\boldsymbol{u}$ | = | air velocity, $m \cdot s^{-1}$ |
| $V$ | = | voltage, V |
| $V_c$ | = | Corona onset voltage, V |
| $\varepsilon_0$ | = | relative permeability, $C \cdot V^{-1} \cdot m^{-1}$ |
| $\eta$ | = | efficiency |
| $\Theta$ | = | thrust-to-power ratio, $N \cdot W^{-1}$ |
| $\mu$ | = | ion mobility, $m^2 \cdot V^{-1} \cdot s^{-1}$ |
| $\rho_g$ | = | air density, $kg \cdot m^{-3}$ |
| $\rho$ | = | charge density, $C \cdot m^{-3}$ |
| $\phi$ | = | electric potential, V |
| $\Psi$ | = | thrust per unit surface, $N \cdot m^{-2}$ |

*Ph.D. Student.
†Researcher, DR-CNRS.
‡Assistant Professor.

## I. Introduction

IN THE past decades, electrohydrodynamic (EHD) thrusters have been popularized with the lifter or "ionocraft" concept. It consists of a light frame supporting two electrodes connected to a high dc voltage supply. At sufficiently high voltages, the device takes off without the help of any mechanical part. This phenomenon relies on the electrostatic air acceleration known as ionic wind.

Ionic or electric wind occurs in atmospheric air when a high-voltage is applied between two asymmetric electrodes. A typical electrode configuration consists of two spaced parallel cylinders having significant diameter difference; this is the wire-to-cylinder case. At the surface of the sharp electrode, the electric field strength exceeds the air breakdown strength. Beyond that threshold, surrounding electrons acquire enough energy to ionize air molecules; this is part of the Townsend breakdown mechanism detailed in [1]. The electric breakdown of the air around sharp electrodes is known as the corona discharge, which can be positive when it occurs at the highest electric potential electrode (anode) and negative when it occurs at the lowest electric potential electrode (cathode). Whatever the polarity, the created ions are strongly accelerated by the electric field in the so-called drift region from the emitting electrode (the wire) to the collecting one (the cylinder). On their way, they collide with neutral air molecules. The momentum transfer during collisions is responsible for the airflow acceleration referred to as ionic wind. And finally from the action–reaction principle, a force is exerted on the electrodes; this is the so-called electrohydrodynamic thrust.

The first results on electric wind were brought forth in 1961 by Robinson [2], who measured velocities up to 4 $m \cdot s^{-1}$. He also found an electric-to-kinetic energy conversion efficiency lower than 1%. Since then, electric wind has been measured by different groups [3–6], and it has never exceeded [7] 10 $m \cdot s^{-1}$, and the efficiency hardly reached 1.7% [8]. The maximum velocity of the ionic wind can be increased by using multistage electrode configurations [9]. It must be noted that the efficiency was always measured in the absence of external airflow, whereas it can be inferred from [10,11] that ambient flow speed would increase it.

EHD devices have been much investigated for their potential applications as flow actuators. Because they do not use any mechanical moving parts, they are of great interest for small-size applications, for example cooling devices [12] or electrosprays [13]. Moreover, their simplicity and fast response make them attractive as they directly convert electric energy into kinetic. During the past

decade, EHD has undergone a growing interest in aerodynamic active flow control around airfoils [14]. The so-called dielectric barrier discharge (DBD) actuator is still an active area of research [15]. DBD actuators have demonstrated their ability to prevent the boundary-layer detachment on airfoils at moderate Reynolds number (i.e., $Re < 10^6$) but hardly affect the flow at higher Reynolds number. Many experiments [16] and fully coupled numerical computations [17,18] were carried out to solve the fluid dynamic, ion chemistry as well as transport in time-dependant electric fields.

The most salient aspect of EHD we are interested in here is the propulsive force applied on electrodes resulting from ions acceleration. This phenomenon was first reported in 1928 by Brown [19,20] and more deeply explored by the seminal investigation of propulsive EHD carried out by Christenson and Moller [21]. Despite the poor efficiency previously mentioned, further investigations have been pursued throughout the years [22,23]. These studies concluded that the thrust density was too low to propel conventional aircraft and that the efficiency would strongly decrease with altitude. However, significant improvements are possible [5,24–27] using adequate electrode shapes and arrangements. Furthermore, Masuyama and Barret [24] recently highlighted the fact that one relevant parameter for comparing in-atmosphere propulsive systems is the specific power consumption. Simple experimental EHD thrusters were then found to reach more than 20 mN/W [24], a value compatible with operating conditions of electrical aircraft, which reopened the issue of EHD propulsion practical interest.

This work aims to quantify the performances of an EHD thruster and investigate more deeply their practical interest. Section II.A is dedicated to a simplified one-dimensional theory of EHD thrusters. The relationship between the time-averaged current and thrust is derived and the efficiency is discussed in Sec. II.B. Experimental measurements are compared to the requirements of ultralight aircraft (ULA) in Sec. II.C. Section III summarizes the experimental results and compares them to the one-dimensional theory predictions. Furthermore, a comparison is drawn between our experimental data and previous measurements to showcase high sensibility to the surrounding environment. Finally, Sec. IV is devoted to the analysis of the aerodynamic drag force applied on the collecting electrodes.

## II. General Considerations

The following simple one-dimensional model has been widely applied to EHD thrusters to predict trends and scaling that can be tested.

### A. One-Dimensional Theory

Recent experiments [5,24,25] widely confirm the trends of the EHD propulsion theory derived by Christenson and Moller [21] in 1967. Inside the drift region, the charge density $\rho$ is only due to ions. Ion velocity originates from two distinct contributions: a convective one from fluid velocity $\boldsymbol{u}$ and a drift one from electroconvection velocity $\mu\boldsymbol{E}$, where the ionic mobility $\boldsymbol{\mu}$ depends on moisture and pressure [28,29], and $\boldsymbol{E}$ is the electric field [30,31]. Ionic velocity is given by

$$\boldsymbol{v} = \boldsymbol{u} + \mu\boldsymbol{E} \tag{1}$$

whereas current density is

$$\boldsymbol{j} = \rho(\boldsymbol{u} + \mu\boldsymbol{E}) \tag{2}$$

The volumetric force $\boldsymbol{f}$ applied on the fluid is equal to the electrostatic Coulomb force applied by the electrodes on the ions:

$$\boldsymbol{f} = \rho\boldsymbol{E} \tag{3}$$

Thus, the net force $\boldsymbol{F}_{\text{EHD}}$ applied over a volume $\mathcal{V}$ of fluid and the net current $I$ flowing through a control surface $S$ are

$$\boldsymbol{F}_{\text{EHD}} = \iiint_{\mathcal{V}} \rho\boldsymbol{E}\,\mathrm{dv} \tag{4}$$

$$I = \iint_{S} \boldsymbol{j}\,\mathrm{ds} \tag{5}$$

The thrust $\boldsymbol{T}$ is then the opposite of $\boldsymbol{F}_{\text{EHD}}$. Let us now simplify the problem to a constant charge density and constant electric field. In this case, $E = -\nabla\phi = V/d$, where $d$ is the length of the drift region, and $V$ is the applied voltage. The input electric power is written $P_e = VI$, the current is $I = \rho S(u + \mu E)$, and the thrust is $T = \rho E\mathcal{V}$. Thus, the thrust-to-power ratio $\Theta = T/P_e$ and propulsive efficiency $\eta = (T \cdot u)/P_e$ can be expressed as the flow velocity and the drift velocity:

$$\Theta = \frac{1}{u + \mu E} \tag{6}$$

$$\eta = \frac{u}{u + \mu E} \tag{7}$$

More general formulas were derived in 1962 by Stuetzer [32] and more recently by Kim et al. [33]. With typical experimental data, $V \approx 20$ kV and $d \approx 2$ cm, so that $E \approx 10^6\ \mathrm{V \cdot m^{-1}}$ and $\mu = 2 \cdot 10^{-4}\ \mathrm{m^2 \cdot V^{-1} \cdot s^{-1}}$, we obtain a drift velocity of 200 m/s. With ambient flowfield $u = 50$ m/s, the thrust-to-power ratio reaches $4\ \mathrm{N \cdot kW^{-1}}$ with a 20% efficiency. As a comparison, according to Masuyama and Barrett [24], typical turbojet engines deliver $2.5\ \mathrm{N \cdot kW^{-1}}$ effectiveness at sea level, where the input power is derived from the specific fuel consumption. Our experimental measurements for zero ambient flow speed ($u = 0$) have shown that $\Theta$ can reach more than $20\ \mathrm{N \cdot kW^{-1}}$ at low voltage, but this is obviously at the cost of low thrust. This simple analysis indicates that the drift velocity must be lowered to increase performance. This can be achieved by two means: decreasing the ion mobility or lowering the electric field.

### B. Corona Discharge Assumptions

In all EHD thrusters previously considered in the literature, air is ionized by a corona discharge, so that ion species and their mobility are not adjustable. Moreover, the corona discharge is space-charge-limited, which means that the generated charge density is limited by the electric field strength and reciprocally. This dependence is responsible for the well-known corona discharge semi-empirical law in the low current approximation, which can be found in [31,34]:

$$I = CV(V - V_c) \tag{8}$$

where $I$ (amperes) is the current, $C$ is an empirical constant depending on electrodes geometry, and $V_c$ (in volts) is the corona inception voltage. A corona discharge relies on a high electric field to generate ions so that it does not allow efficient energy conversion according to Eq. (7). Moreover, neglecting the flow velocity $\|\boldsymbol{u}\| \ll \|\mu\boldsymbol{E}\|$ and assuming a constant mobility $\mu$ allows some simplifications in the theoretical derivation of thrust and thrust-to-power ratio; the charge conservation law in the drift region $\nabla \cdot \boldsymbol{j} = 0$ becomes $\nabla \cdot \boldsymbol{\rho E} = 0$. The flux of force is therefore conserved in a current tube. Gilmore and Barrett [27] use this property to compute the force and the thrust-to-power ratio of one current tube, starting from the emitter and ending at the collector:

$$T_{\text{tube}} = \frac{I_{\text{tube}} d_{\text{drift}}}{\mu} \tag{9}$$

$$\Theta_{\text{tube}} = \frac{d_{\text{drift}}}{\mu V} \tag{10}$$

Those results are general and do not depend on the electric field shape [27]. More precisely, thrust and thrust-to-power of one current tube do not depend on the ion path (electric field lines) but only on the projection $d_{\text{drift}}$ of this path along the thruster axis; see Fig. 1. In the case of electrodes having a small extension along the thruster axis, the mean path projection of all current tubes is equal to the distance $d$ between the electrodes. Then, the net thrust can be computed by integrating the contribution of each current tube:

$$T_{\text{th}} = \frac{I d_{\text{drift}}}{\mu} \tag{11}$$

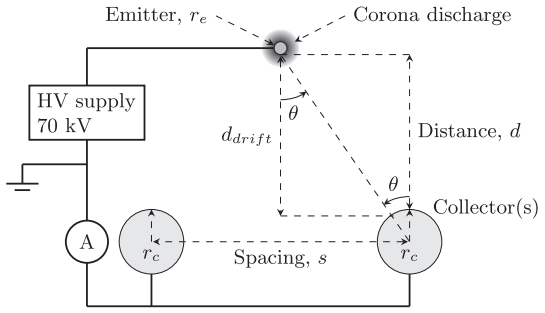


**Fig. 1 Electrode size and electrical wiring for a positive discharge.**

We introduce the thrust density $\Psi$, which is the net thrust per unit gap distance $d$ and per unit electrode length $l$:

$$\Psi \equiv \frac{T}{ld} = \frac{i}{\mu} \tag{12}$$

where $i = I/l$ (in amperes per meter) is the current per unit electrode length. A simple approximate relationship between $\Theta$ and $\Psi$ can be derived. Following [5], we assume that we operate far from the inception point $V_c \ll V$ so that $i \approx CV^2/l$. Substituting into Eqs. (10) and (12) leads to

$$\Theta = \frac{d}{Vi}\Psi \approx \frac{d}{\mu^{3/2}}\sqrt{\frac{C}{l\Psi}} \tag{13}$$

A similar relationship was derived in [5]. It failed to predict accurately $\Theta$ at low voltage, but did however provide a good estimation of the influence of parameters. In simple geometries, such as concentric cylinders [31,35] or wire to cylinder [5], the constant $C$ is proportional to $l\mu\varepsilon_0/d^2$, leading to

$$\Theta = \frac{\sqrt{\varepsilon_0 C_0}}{\mu}\frac{1}{\sqrt{\Psi}} \tag{14}$$

$$i = \mu\varepsilon_0 C_0 E(E - E_c) \tag{15}$$

where $C_0 = C \cdot d^2/(l\mu\varepsilon_0)$ is a nondimensional constant nearly independent of $d$; $E = V/d$; and $E_c = V_c/d$. It is noteworthy that, with this formalism, thrust-to-power ratio does not depend on $d$ at fixed $\Psi$, and $i$ depends only on the mean electric field $V/d$.

### C. Application to Aerial Propulsion

Although the thrust generated by EHD devices has already been measured, only a few studies compare it to the net thrust required for aerial propulsion. Wilson et al. [22] estimate that reaching a thrust density of $20\ \mathrm{N \cdot m^{-2}}$ (frontal area) and an effectiveness of $20\ \mathrm{N \cdot kW^{-1}}$ simultaneously is necessary for practicable applications besides any justification given. In the following, we compute the thrust per unit area required to fly an electric aircraft and compare it to the thrust density delivered by an experimental thruster. We choose three different types of light aircraft, whose characteristics are gathered in Table 1, and we assume that every aircraft carries a 90 kg additional payload (e.g., a pilot). We note that $m_a$ is the mass of the aircraft with its pilot. Considering an aircraft in horizontal flight, the net drag $D$ depends on the weight and the lift-to-drag ratio as follows:

**Table 1 Aircraft parameters**

| Aircraft type | $m_a$, kg | $L/D$ | $S_w$, m$^2$ | $E^*$, (W · h)/kg |
|---|---|---|---|---|
| Ultralight (Sinus[a]) | 310 | 25 | 27 | 190 |
| Electric glider (Taurus[a]) | 264 | 41 | 26.6 | 190 |
| Solar aircraft (Solar Impulse 2[b]) | 1757 | 34 | 540 | 260 |

[a]Data available online at http://www.pipistrel.si [retrieved February 2016].
[b]Data available online at http://www.solarimpulse.com [retrieved February 2016].

$$D = \frac{Mg}{L/D} \tag{16}$$

where $M$ is the net mass of the aircraft:

$$M = m_a + m_b \tag{17}$$

where $g$ is the gravity acceleration, $L/D$ is the lift-to-drag ratio, and $m_b$ is the mass of battery. To sustain horizontal flight, the propulsion system must generate a thrust balancing drag $D$. The propulsive system is characterized by its thrust-to-power ratio $\Theta$, which determines its power consumption: $P_e = D/\Theta$. Then, the amount of needed battery $m_b$ for a given flight duration $\mathcal{T}$ can be determined as follows:

$$m_b = \frac{P_e \mathcal{T}}{E^*} = \frac{\mathcal{T} D}{\Theta E^*} \tag{18}$$

$E^*$ is the energetic density of the batteries. Combining Eqs. (16–18), we obtain the thrust required for horizontal flight as a function of the thrust-to-power ratio for a given flight duration:

$$T = \frac{m_a g}{((L/D) - (\mathcal{T} g/\Theta E^*))} \tag{19}$$

From now on, the propulsive system is assumed resulting from independent distributed electrodes covering the whole external surface of the aircraft, $S_w$, and integrated as a wire-to-wire plasma actuators [14]. In this highly idealized configuration, the thrust density $\Psi$ is given by

$$\Psi = \frac{m_a g}{S_w((L/D) - (\mathcal{T} g/\Theta E^*))} \tag{20}$$

Therefore, it is now possible to compare the theoretical thrust density required to fly the aircraft given by Eq. (20) to the experimental thrust density produced by the electrodes. The results are provided in Fig. 2 [(1, solid line) ULA whose thermal engine was replaced by batteries. (1, dashed line) same ULA with a 30 kg lighter pilot. (1, dotted line) same ULA with improved battery energetic density $E^* = 260\ (\mathrm{W \cdot h})/\mathrm{kg}$. (1, dash-dotted line) ULA with improved glide ratio $L/D = 30$. (2) Electric glider: the drag/surface ratio corresponding to a mass of 396 kg including 41 kg of batteries (actual mass) is marked by (−−−). (3) Solar Impulse 2: the drag/surface ratio corresponding to a mass of 2300 kg including 633 kg of batteries (actual mass) is marked by (−−−). (4) Experimental curve: $r_e = 25\ \mu$m, $d = 2$ cm, $r_c = 5$ mm, and RH = 41%. The aircraft parameters are given in Table 1] and are compared with our experimental measurements (see Sec. III.B).

The glide ratio of Solar Impulse 2 is estimated according to the altitude loss during nighttime, and its wetted area is approximately twice the solar cell surface ($2 \times 270\ \mathrm{m^2}$). For the other electrical aircraft, wetted areas are estimated from the wing surface: $S_w = 2 \times S_{\mathrm{wing}} + S_{\mathrm{fuselage}}$, where a surface of $S_{\mathrm{fuselage}} = 2\ \mathrm{m^2}$ is assumed for the fuselage. As expected, a high means less battery needs, so that the required thrust is slightly lower. On the contrary, flying with $\Theta \leq 3\ \mathrm{N \cdot kW^{-1}}$ seems unrealistic because battery mass reaches half aircraft net mass. Not surprisingly, the thrust density provided by this not optimized experimental thruster does not reach the needs of classical aircraft (ULA and glider) even with strong improvements in terms of glide ratio, structural mass, or battery energetic density. However, as can be seen in Fig. 2, the thrust density that can be reached, although smaller, is not negligible compared to the one required. At least, it shows that EHD thrust can provide interesting effects. Theoretically, it could even provide enough thrust to propel Solar Impulse 2 for 1 h. This shows that a low-speed aircraft with a wide wetted surface combining all the preceding improvements could possibly be propelled by EHD means. Whether this statement can reach practical interests still remains dubious. Indeed, it should be noted that the integration of the electrodes at the surface of the wings could reduce the thrust density because half of

the volume between the electrodes would be under the surface of the airfoil and because of skin friction of the ionic wind along the wing wall. The efficiency of the electric energy conversion process by ion collisions is weak, and this remains a serious drawback of EHD systems, even if Eq. (7) indicates ways that it could be improved. Furthermore, the thrust level is expected to decrease with altitude because of lower air density and higher ionic mobility [2,23]. System reliability, ambient airflow effects on the discharge, and security are still important and unsolved open issues. Although EHD propulsion is far from industrial application, it nevertheless exhibits some distinct advantages worth considering; it does not involve any mechanical moving parts, the propulsive system can be small, and it is noise-free. Furthermore, it directly interfaces with battery energy storage at low energy conversion loss, as opposed to the conversion loss associated with electromechanical propulsion systems. Given the low thrust generated, it is most likely to appear possibly useful, as a distributed propulsion system.

## III. Experimental Investigation

The following experiment was inspired by previous work [5,24,25] using similar setups to measure thrust and current. The electrode shape and arrangement was investigated by varying both the emitter and the collector radius ($12.5 \leq r_e \leq 100$ $\mu$m and $1.5 \leq r_c \leq 5$ mm; if not specified: $r_e = 25$ $\mu$m and $r_c = 5$ mm), the gap length ($2 \leq d \leq 6$ cm) and the use of two collecting electrodes with varying spacing ($0 \leq s \leq 10$ cm; if not specified, only one collector is used: $s = 0$ cm). This last point highlighted a possible aerodynamic drag effect on the collecting electrodes. Figure 2 summarizes these geometrical parameters.

### A. Experimental Setup

The EHD thruster was composed of one emitting tungsten wire and one or several collecting steel cylinders. The electrodes length was $l = 39$ cm, and they were supported by a $40 \times 40$ cm polytetrafluoroethylen (PTFE) frame. To avoid bending or vibrations, the tip of the emitting wire is wound around Nylon screws to ensure sufficient tension. Air relative humidity (RH) and temperature were recorded with a HL-1D sensor. The PTFE frame was hung by Nylon wires to a precise balance ME3002 ($0.01g$) as shown in Fig. 3. The distance between the high-voltage electrode and the balance was at least 50 cm. The digital scale was supported by a 2-cm-thick polyvinyl chloride (PVC) plate of the same dimensions as the scale. The whole suspended frame weighed around 2.7 kg. The maximum registered thrust was around $-10g$. The high voltage (HV) power supply Iseg HP700505p provided a positive voltage up to 70 kV. Particular care was taken in the wiring to insure that the weight and the stiffness of the cables do not affect the measurements. The connection was ensured by a thin horizontal wire of the same type as the emitting wire. Flow velocity fluctuations were recorded with a DANTEC P11 hot-wire probe. The sampling frequency was 1 kHz, and the acquisition window lasted 60 s.

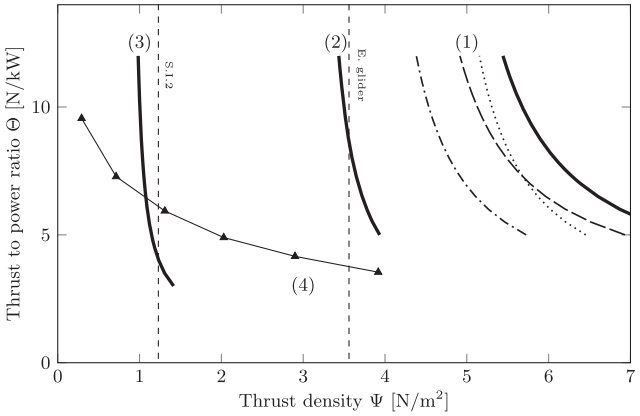


**Fig. 2 Thrust-to-power ratio vs required thrust density [Eq. (20)] for a 1 h horizontal flight and for different aircraft characteristics.**

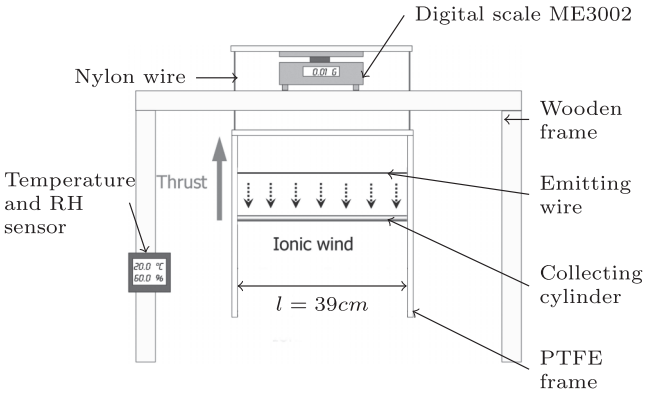


**Fig. 3 Experimental thrust measurement. The minimum distance between balance and high voltage was 50 cm.**

The power supply displays the value of the applied voltage with a very satisfactory accuracy when compared to the voltage measured with a high-voltage probe TESTEC TT-HVP40. The relative measurement difference is less than $2 \cdot 10^{-3}$ for voltages higher than 10 kV. The digital current display precision is less satisfactory for low currents, and so a LUTRON DM9090 multimeter is connected to ground to measure the current. This dual-current measurement highlighted a current difference, referred to as the "current leakage", between the high-voltage branch and ground. This current leakage depends only on the applied voltages. It is more noticeable for large electrode gap $d$ because, at a fixed current, this required a higher voltage. The current leakage proportion was typically less than 10% for gap values below 4 cm but could reach more than 50% for a 14 cm gap. This current leakage (see Fig. 4) is due to the thin connecting wires around which corona discharge occurs. Replacing these wires by isolated wires reduces current leakage but simultaneously disabled thrust measurement because of strong stiffness. Consistent with [5,25], the presented current is measured in the grounded part of the circuit. The measurement procedure is the following: high voltage is set to the desired value for at least 5 s, and then data are recorded during 20 s at a sampling rate of 20 Hz before being averaged.

During the first trial, we observed that the thrust measurement could be affected by parasite electrostatic forces due to the charging of the environment; before any thrust measurement, the scale was calibrated to zero. Then, high voltage was switched on during 20 s and finally turned off. Instead going back to zero, the scale indicated a negative thrust (directed downward) slowly decreasing in time. It typically took between 30 s and 1 min for the measured force to reach zero again. The decreasing time and amplitude of this anomalous force also depended on the floor material below the PTFE frame: wood, concrete, PVC plate, or antistatic foam. To avoid such sensitivity, both the digital scale and the electrode frame were elevated until this effect became negligible and no floor material dependence could be measured. The emitter was 85 cm above the

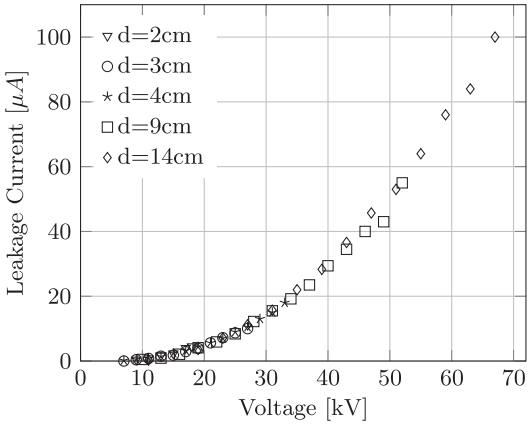


**Fig. 4 Leakage current vs voltage for different electrode gap.**

floor and at least 50 cm below the digital scale, whose metallic body was grounded. The lowest part of the PTFE frame was 50 cm above the floor. Thrust measurements have been voluntary restricted to small distances and relatively low voltages, below 40 kV.

### B. Results

The experimental results are presented in terms of thrust, thrust density, applied voltage, current per unit length, and thrust-to-power ratio. The measurements are made without ambient flow. The applied voltage is positive, so that a positive corona discharge occurs at the emitter.

A back-discharge can arise when the electric field strength at some points on the collector approaches the dielectric strength of the air, generating negative ions traveling backward. Most of the time, the backdischarge is located at the tips of the cylinder. This parasite current is responsible for the so-called bilinear performance degradation described in [24]. It can be detected because current becomes unstable with noise emission. To avoid backdischarge, voltage is limited for all measurements except in the special case of $d = 9$ cm for illustrating its negative impact. In this study, the practical maximum thrust density limited by spark formation is not reached.

#### 1. *Comparison with Previous Measurements*

Measurement of thrust, voltage, and current may show sensible variation according to changing atmospheric parameters or electrostatic charging of the surrounding area, which generates parasite forces. They are compared with similar previous experiments in Fig. 5. The case of a) and b) corresponds to Figs. 9 and 10 in the article [5]: $r_e = 12.5$ $\mu$m, $r_c = 1.5$ mm, $d = 2$ cm, Tungsten wire. Whereas cases c) and d) compare the data of [25]: $r_e = 25$ $\mu$m, $r_c = 5$ mm, $d = 3$ cm, copper wire.

The T-V and I-V curves are very similar. Only a slight difference between [5] and the presented results is noticeable.

We found, however, a significant difference with [24] results, typically more than 50% for voltages higher than 30 kV (not shown). However, we could not reproduce exactly the same configuration as [24] ($r_e = 100$ $\mu$m, $r_c = 3.15$ mm, $d = 9$ cm) and used a bigger collector ($r_c = 5$ mm), which should have provided a higher performance according to [5]. Nevertheless Masuyama and Barret's thrust and current [24] are at least twice higher. Furthermore, Masuyama and Barret [24] measured the current directly with the power supply, and so leakage current (Sec. III.A) might explain the current difference but still does not explain thrust differences.

#### 2. *Distance Effect*

The distance between the electrodes has two antagonistic effects on performance. First, the strength of the electric field, which also drives the injected charge density, is determined by the voltage gradient. Second, the net thrust is proportional to the volume of the drift region. Thus, the distance $d$ strongly affects the net EHD thrust. But using quantity rescaled with $d$, it is noteworthy that all experimental curves provided in Figs. 6a and 6b collapse whatever the distance. This confirms the weak dependence of $C_0$ on $d$. We found $\mu\varepsilon_0 C_0 = 1.27 \cdot 10^{-15}\mathrm{A \cdot m^{-1} \cdot V^{-2}}$, with a Tungsten wire and the following electrode's geometry: $r_e = 25$ $\mu$m, $r_c = 5$ mm and $s = 0$ cm. However, this collapse is not perfect, especially at low electric fields because the corona inception field $E_c = V_v/d$ varies with $d$ (see Table 2).

As shown in Fig. 6, thrust–voltage (T-V) and current–voltage (I-V) curves have a very similar shape. This is due to the linear relationship between the current and the EHD forces illustrated in Fig. 6c and predicted by Eq. (12). However, the effective mobility, given by the slope of the $\Psi$–$i$ curve, does not fall within prediction range; the current conversion into thrust is less efficient than expected. The variations of ions mobility in air with pressure, temperature, and humidity (between 1.6 and 2.2 $\mathrm{cm^2 \cdot V^{-1} \cdot s^{-1}}$ depending on air humidity [28]) are not sufficient to explain the value of the effective mobility, close to 2.66 $\mathrm{cm^2 \cdot V^{-1} \cdot s^{-1}}$, obtained in our experiments. This point, related to the drag of the collector, will be discussed later in Sec. IV.

For large gap values, the applied voltage is limited by the inception of the negative discharge at the collector. The backdischarge current was voluntary recorded only for distance $d = 9$ cm. It causes a slope change in the $\Psi$–$i$ characteristic and a drop of $\Theta$. The thrust density is not affected by the backdischarge. This undesired power consumption can be limited by decreasing the electric field at the tip of the collector, for example by increasing the collector radius up to a limit (see Sec. III.B.4).

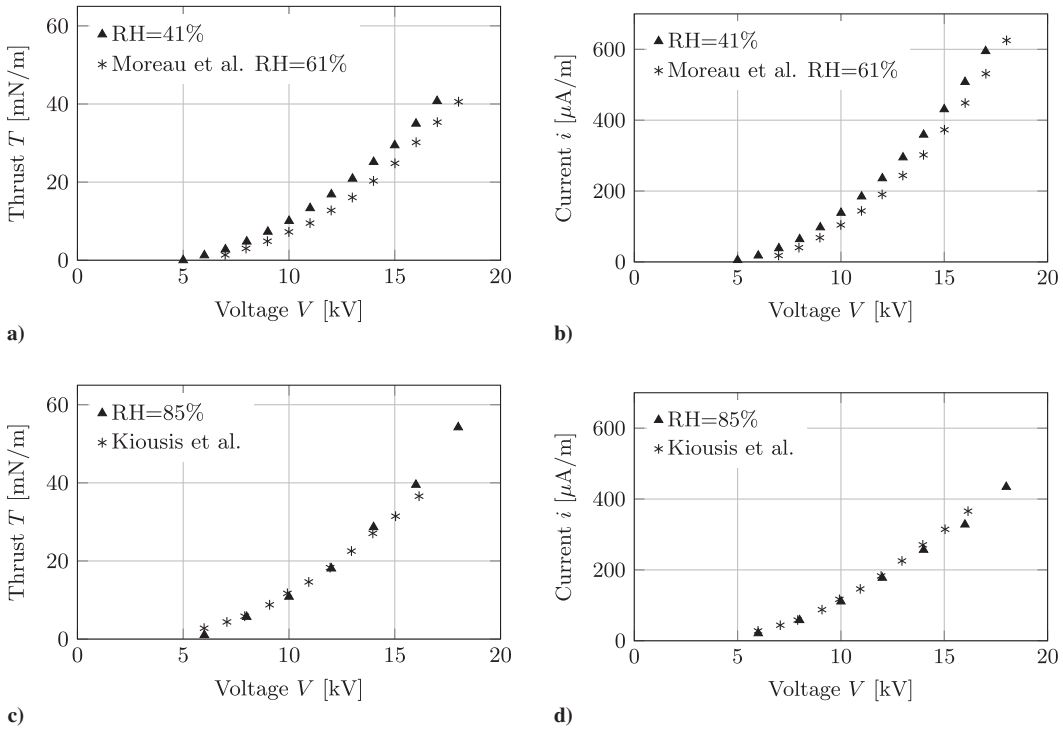


**Fig. 5 Comparison of measurement from literature (∗ symbol) with ours (▲) for a positive discharge. a–b) data of [5]. c–d) data of [25].**

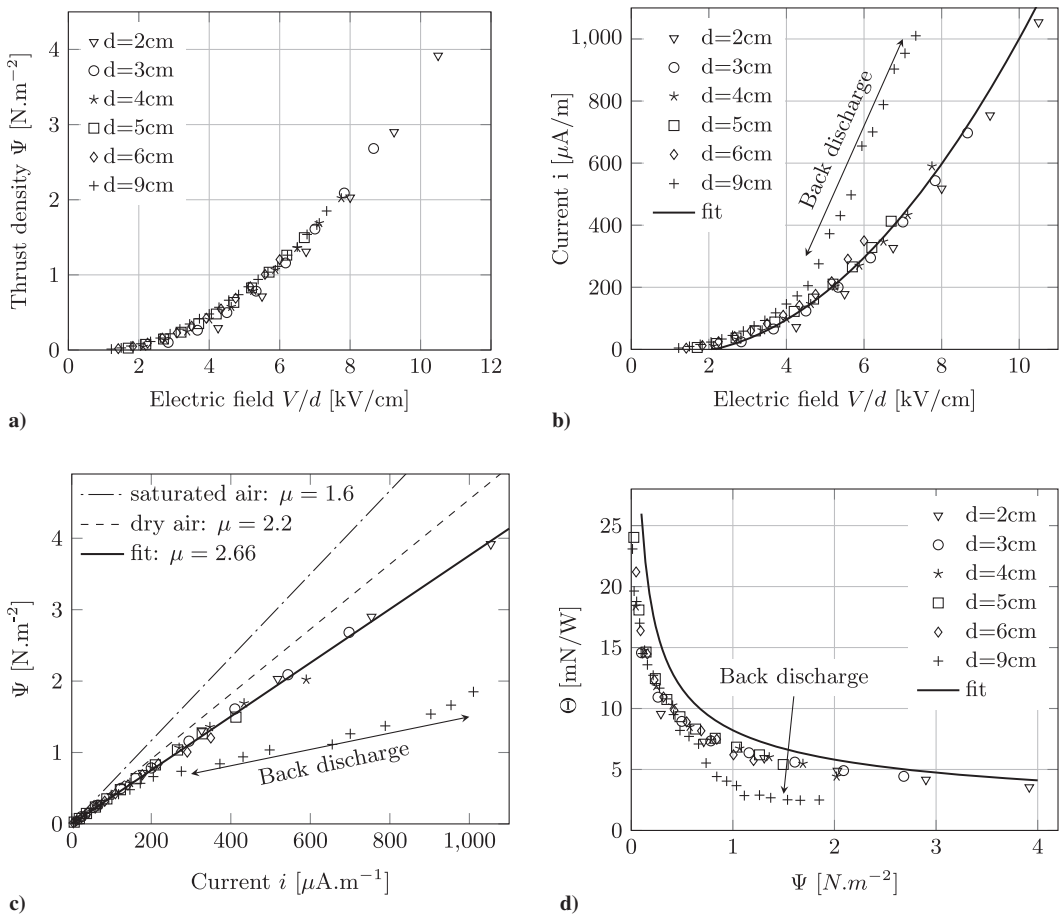


**Fig. 6 Representations of a) thrust density vs electric field $V/d$; b) current vs electric field. Case $d = 4$ cm fitted with Eq. (15): $\mu\varepsilon_0 C_0 = 1.27 \cdot 10^{-15}$ A $\cdot$ m$^{-1}$ $\cdot$ V$^{-2}$ and $E_c = 2.12$ kV $\cdot$ cm$^{-1}$. c) Thrust density vs current, fitted with Eq. (12), mobility in cm$^2$ $\cdot$ V$^{-1}$ $\cdot$ s$^{-1}$. d) Thrust-to-power vs thrust density Ψ, fitted with Eq. (14).**

In previous studies [24–27], increasing the gap between the electrodes at fixed net thrust allowed to reach higher thrust-to-power ratio, but it automatically led to higher voltages. On a practical point of view, our results show that, at fixed thrust density, the distance between the electrodes plays a secondary role. This is both good and bad news. Bad news comes when increasing the gap poorly increases performance but leads to even easier backdischarge. The good news is that the smaller the gap is, the lower the voltage is, without almost performance degradations. A set of serialized small devices with low voltages (with succession of positive and negative discharge) could then reach similar thrust level as a big one associated with a huge voltage.

### 3. *Emitter Radius Effect*

The emitting wire radius must be small compared to the collector so that the electric field reaches its critical inception value only at one electrode. The semi-empirical Peek's formula gives an estimate of the critical electric field $E_{s,c}$ (in kilovolts per millimeter) required at the surface of the wire for corona:

$$E_{s,c} = 3.1 m \delta \left(1 + \frac{0.308}{\sqrt{\delta r}}\right) \tag{21}$$

where $m = 1$ for a smooth wire, $\delta = (298 * p)/T$ with $p$ (in bar) pressure, and $T$ (in kelvins) is temperature. The critical inception voltage $V_c$ can be derived from the surface electric field $E_{s,c}$ using analytical solution for the wire-to-cylinder case [36]. Figure 7a displays the inception voltage versus wire radius. Reducing the emitting wire diameter shifts the Ψ–$V$ and $i$–$V$ curves toward lower voltages because it reduces the corona inception voltage. At fixed thrust, it means less electric power consumption. It is noteworthy that $V_c/d$ (see Table 2) is rather similar to Moreau et al.'s data [26], despite Moreau et al.'s wire being 25 $\mu$m of diameter, and ours is 50 $\mu$m.

### 4. *Effects of Other Parameters*

The influence of other parameters has been tested: discharge polarity, collector radius, and the material of the emitting wire. The entire set of collected data is not presented for the sake of conciseness, but we obtained results similar to previous study [5,25].

One result should, however, be emphasized. Increasing the size of the collecting electrode can increase the thrust at fixed voltage. However, when the size of the collector is further increased, the thrust drops. Moreau et al. [5] find an optimum diameter around 10 mm for a distance of 2 cm. This collector size change leads to an increase or a decrease of the slope of the linear Ψ–$i$ relationship, which should only depend on the ion mobility according to Eq. (12). However, the same behavior can be observed when two collectors are used. Figure 7b shows the anomalous slope variation. A strong variation of the ion mobility or of the drift distance due to various collectors seems unlikely. In the following, we argue that the aerodynamic drag force exerted by the ionic wind airflow on the collecting electrode is responsible for this anomalous slope variation. Quantifying this drag is important because it reduces the efficiency of the thruster.

**Table 2 Comparison of the corona inception field $E_c = V_c/d$ with Moreau et al.'s data [5]**

| $d$, cm | 1 | 1.5 | 2 | 3 | 4 | 5 | 6 |
|---|---|---|---|---|---|---|---|
| $E_c$, kV/cm | — — | — — | 3.15 | 2.31 | 2.12 | 1.70 | 1.62 |
| Moreau $E_c$, kV/cm | 4.8 | 3.6 | 3.05 | 2.5 | 2.2 | — — | — — |

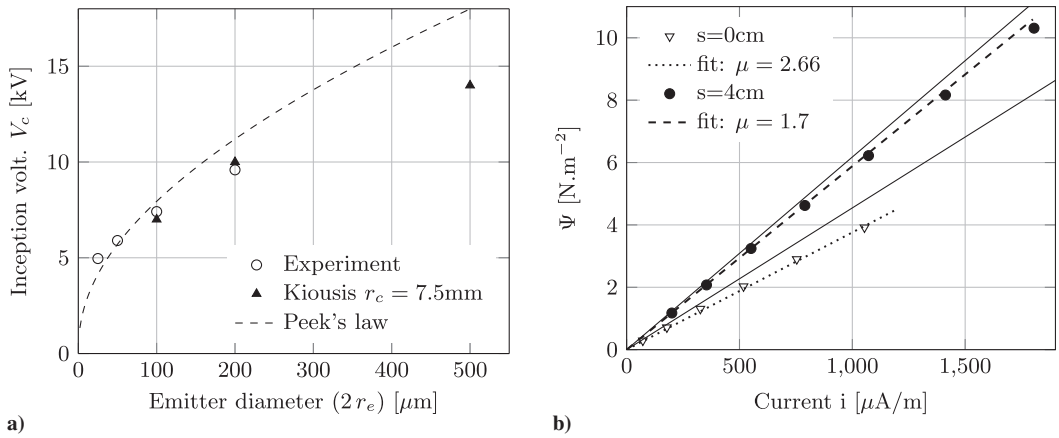


**Fig. 7 a) corona onset voltage vs the emitter diameter ($d = 3$ cm, $r_c = 1.5$ mm). Experimental data compared to [25] and Peek's formula Eq. (21); b) $\Psi$–$i$ curve for different spacing, $d = 2$ cm. Full line for Eq. (12), fitted values of $\mu$ in cm$^2 \cdot$ s$^{-1} \cdot$ V$^{-1}$.**

## IV. Aerodynamic Drag Effect

The determination of the aerodynamic drag of the collectors would, in principle, require velocity profile both upstream and downstream. High voltages prevent the use of measurement probe upstream. Thus, a direct drag measurement is difficult. However, we can provide evidence that such drag exists and influences the measured performances of EHD thrusters.

### A. Ionic Wind Fluctuations

By measuring the ionic wind velocity profile at the collecting electrode with a homemade glass pressure probe, Moreau et al. [5] estimated a thrust 70% higher than the measured one. In the present study, we investigated the flow ($r_e = 25$ $\mu$m, $d = 2$ cm) using a hot-wire probe. Because this kind of probe requires a precise calibration that might be sensible to the electric field and discharge current (sharp edges), no precise quantitative measurement was carried out. However, the low response time of the probe highlighted temporal properties of velocity fluctuations in the collector wake 5 cm downstream, far from the discharge zone. Figure 8a displays the power spectral density (PSD) of signal fluctuations: $e(t)' = e(t) - \bar{e}$ where $\bar{e}$ is the time average. It shows an obvious maximum at frequency $f_{\max}$, which grows linearly with the applied voltage and decreases as the size of the collector increases (Fig. 8b). These time-periodic velocity fluctuations can be related to a vortex shedding instability mechanism. For an ionic wind of 1 m $\cdot$ s$^{-1}$ [5] and a collector diameter of 1 cm, the Reynolds number $Re$ is close to 600 and falls in the range of the well-known von Kármán instability.

The upstream ionic wind velocity cannot be directly measured, but it can be estimated by neglecting pressure and viscous effect in the momentum equation of the fluid:

$$\rho_g u \frac{\mathrm{d}u}{\mathrm{d}x} = \rho E \tag{22}$$

where $\rho_g$ (in kilograms per cubic meter) is the air density. The momentum equation can be integrated on a volume including all EHD forces:

$$\iiint_{\mathcal{V}} \rho E = F_{\mathrm{EHD}} = -T$$

The incoming momentum flow is neglected:

$$\frac{1}{2}\rho_g u(d)^2 \mathcal{S} = F_{\mathrm{EHD}} \tag{23}$$

where $\mathcal{S}$ is the exhaust surface of the integration volume, and $u(d)$ is velocity at the exhaust surface. Because $F_{\mathrm{EHD}} = Id/\mu$ and $I \approx CV^2$, we finally recover the usual ionic wind velocity:

$$u(d) \approx \sqrt{\frac{2dC}{\mathcal{S}\rho_g \mu}} \cdot V \tag{24}$$

This result states that ionic wind varies linearly with applied voltage, as shown in [2]. At low Reynolds number, the dimensionless vortex frequency, the Strouhal number $St$, is nearly constant [37]: $St = u2r_c/f \approx 0.2$. Thus, the frequency of vortex shedding is expected to grow linearly with the airflow velocity as so with voltage, which is in agreement with our measurement Fig. 8b.

Despite no precise velocity measurement having been performed upstream, this experiment highlighted a nonstationary wake, which

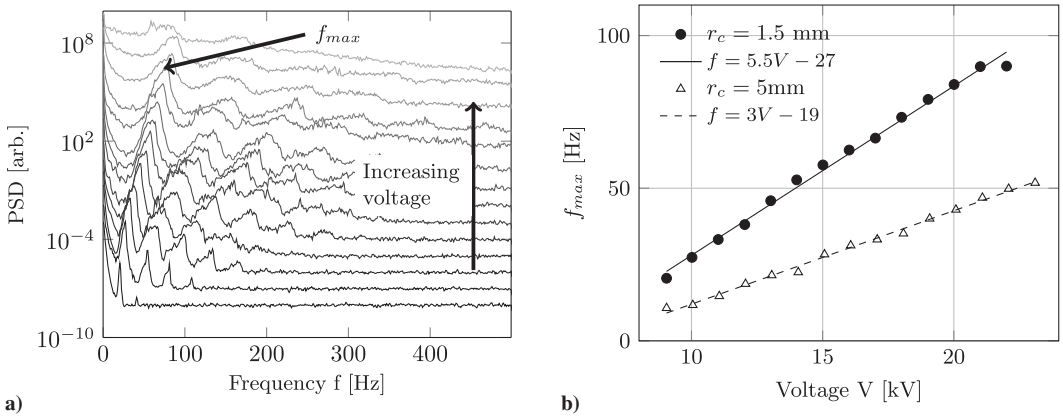


**Fig. 8 a) PSD of signal fluctuations with offset for readability (arbitrary units), and b) evolution of $f_{\max}$ with voltage. Symbols for measurements, continuous lines for linear fit.**

could potentially lead to nonlinear wake interactions in the case of multiple collecting electrodes.

The next part is dedicated to drag estimation and its impact on thruster's performance measurements.

### B. Collector Drag Estimation

A crude estimate of the drag associated with one collector can be obtained using the drag coefficient $C_D$ of a circular cylinder and Eq. (23) leading to

$$D = \frac{1}{2}\rho_g u(d)^2 (2r_c l) C_D = \alpha F_{\text{EHD}} \tag{25}$$

where $\alpha$ is a constant depending on the drag coefficient. Using Eqs. (10) and (11), it is possible to estimate the aerodynamic drag $D$

$$D = T_{\text{th}} - T \tag{26}$$

where $T$ is the measured thrust, and $T_{\text{th}} = I d_{\text{drift}}/\mu$ is the theoretical thrust. Using Eq. (25) and because $F_{\text{EHD}} = T_{\text{th}}$, we can rewrite Eq. (26):

$$\alpha = 1 - T^* \tag{27}$$

where $T^* = T/T_{\text{th}}$ is the nondimensional thrust. $T_{\text{th}}$ highly depends on the choice of the ionic mobility $\mu$, which varies with air humidity and other atmospheric parameters. However, Moreau et al. [5] showed that those variations are relatively limited air relative humidity (RH) when $48 \leq \text{RH} \leq 62\%$. Our measurements were obtained with relative humidity between 45 and 60%. Thus, we decided to choose a single ionic mobility equals to 1.8 $\text{cm}^2 \cdot \text{V}^{-1} \cdot \text{s}^{-1}$ according to precise measurement made in a positive dc corona discharge [38]. Furthermore, the drift distance is chosen so that the angle $\theta$ between the thruster axis and the ions' path is taken into account (see Fig. 2):

$$d_{\text{drift}} = d + (1 - \cos\theta) \cdot r_c \tag{28}$$

Comparing various configurations to each other provides evidence that aerodynamic effects are not negligible and highly depend on the electrode position. Figure 9 shows that the use of several collectors can increase the performance, which is in agreement with previous observations [22,26]. When the nondimensional spacing is lower than 2, the experimental performances are poor: only 70% of the expected thrust and thrust-to-power ratio. This is very probably due to an increase of the drag when the collecting electrodes are placed on the thruster axis, where ionic wind is stronger. However, when the spacing is big enough, it is possible to nearly reach the theoretical predictions. The optimum nondimensional spacing depends on the gap size but is in the range [4,8]. On the contrary, for a wide spacing, the airflow velocity seen by the collectors is lower. At very large spacing, performance drops again, as can be expected from the deflections of the electric field lines driving the flow. A secondary effect is noticeable as the distance increases; the performances are lower when the gap size increases. This is possibly due to a widening of the velocity profile resulting in an increasing drag.

As illustrated on Fig. 10a, the dimensional drag varies almost linearly with $d$, which is in agreement with the variation of the ionic wind velocity with $d$ [Eq. (24)] and the very weak variation of the drag coefficient of a cylinder for the range of Reynolds numbers obtained in the experiments ($Re \sim 200$). The drag also increases with the spacing, even if, for unknown reason, the case $s = 10$ cm seems to behave differently. The nondimensional drag $\alpha$ slowly increases

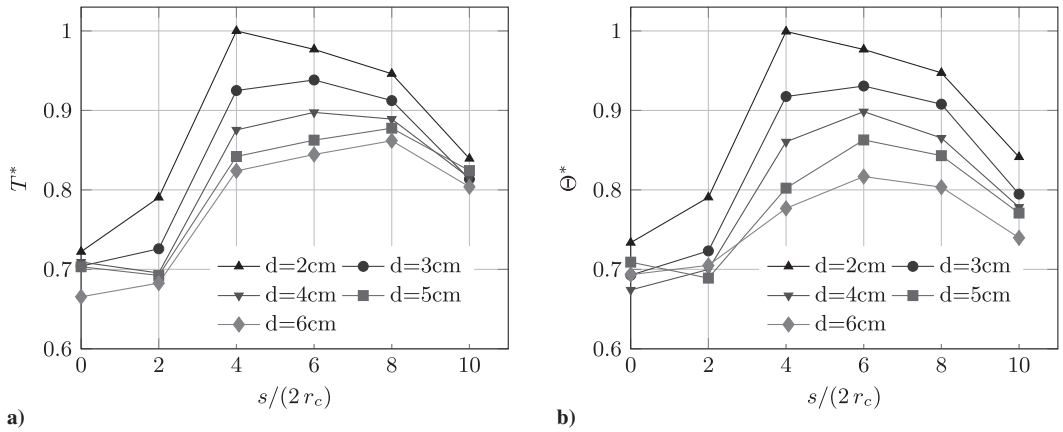


**Fig. 9 Representation of a) $T^*$ vs spacing at fixed current $I = 250\ \mu\text{A} \cdot \text{m}^{-1}$ (interpolated data), and b) $\Theta^* = \Theta/\Theta_{\text{th}}$ vs spacing at fixed thrust $T = 26\ \text{mN} \cdot \text{m}^{-1}$ (interpolated data).**

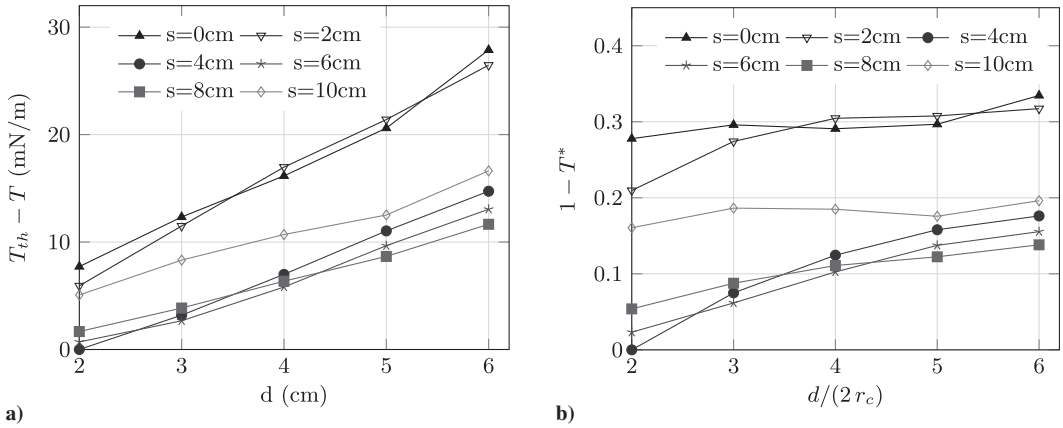


**Fig. 10 Representations of a) collector(s) estimated drag as a function of distance for various spacing, $i = 250\ \mu\text{A} \cdot \text{m}^{-1}$, and b) nondimensional drag $\alpha$ as a function of the nondimensional distance at fixed current $i = 250\ \mu\text{A} \cdot \text{m}^{-1}$.**

with $d$. For small spacing, it seems to be independent on the distance, indicating that the drag coefficient remains unchanged. For larger spacing values, a small dependence is observed. This effect can be related the variation of the velocity profile upstream of the collectors with the geometric configuration ($s$ and $d$).

## V. Conclusions

This study focused on the propulsive electrohydrodynamic (EHD) effect of a simple wire–cylinder electrode configuration and its potential use for aerial propulsion. The classical model of EHD propulsion is presented, and the renewed interest for this propulsion device due to its thrust-to-power ratio is explained. Simple considerations on aircraft performance confronted with experimental results provided evidence that EHD may have interesting unexplored potential for very light, low-speed aircraft propulsion. Whereas most of the presented experiments confirm trends already found in previous studies, some new results were highlighted. First, comparison of the present measurements with other studies showed that experimental bias must be carefully handled: leakage current and parasite thrust errors are not negligible. Second, all data were rescaled according to the gap $d$, and the thrust per unit distance $\Psi$ was introduced. On this point of view, the distance between the electrodes does not strongly affect the EHD performances. The practical consequence is that working with small devices at low voltages in a series must be theoretically as efficient as working with only one very high-voltage device. Finally, the flow behind the collector exhibited fluctuations typical of a vortex shedding like instability. No precise ionic wind measurements were performed, but an indirect drag estimation based on various electrodes configurations showed that aerodynamic effects are not negligible.

Further measurements on flow dynamic around the electrodes are necessary to better quantify the drag force exerted on the collector. This could be achieved by means of nonintrusive flow measurement methods such as laser Doppler anemometry or particle image velocimetry.

## Acknowledgments

N. Monrolin thanks Region Occitanie and Centre National d'Études Spatiales (CNES) Launcher Directorate for financial support. This research has been funded by CNES research contract 5100015475.

## References

[1] Fridman, A., Chirokov, A., and Gutsol, A., "Non-Thermal Atmospheric Pressure Discharges," *Journal of Physics D: Applied Physics*, Vol. 38, No. 2, 2005, p. R1. doi:10.1088/0022-3727/38/2/R01

[2] Robinson, M., "Movement of Air in the Electric Wind of the Corona Discharge," *Transactions of the American Institute of Electrical Engineers*, Vol. 80, No. 2, 1961, pp. 143–150.

[3] Yabe, A., Mori, Y., and Hijikata, K., "EHD Study of the Corona Wind Between Wire and Plate Electrodes," *AIAA Journal*, Vol. 16, No. 4, 1978, pp. 340–345. doi:10.2514/3.7528

[4] Rickard, M., Dunn-Rankin, D., Weinberg, F., and Carleton, F., "Characterization of Ionic Wind Velocity," *Journal of Electrostatics*, Vol. 63, Nos. 6–10, 2005, pp. 711–716. doi:10.1016/j.elstat.2005.03.033

[5] Moreau, E., Benard, N., Lan-Sun-Luk, J.-D., and Chabriat, J.-P., "Electrohydrodynamic Force Produced by a Wire-to-Cylinder DC Corona Discharge in Air at Atmospheric Pressure," *Journal of Physics D: Applied Physics*, Vol. 46, No. 47, 2013, Paper 475204. doi:10.1088/0022-3727/46/47/475204

[6] Mizeraczyk, J., Podlinski, J., Niewulis, A., and Berendt, A., "Recent Progress in Experimental Studies of Electro-Hydrodynamic Flow in Electrostatic Precipitators," *Journal of Physics: Conference Series*, Vol. 418, 2013, Paper 012068.

[7] Colas, D. F., Ferret, A., Pai, D. Z., Lacoste, D. A., and Laux, C. O., "Ionic Wind Generation by a Wire–Cylinder–Plate Corona Discharge in Air at Atmospheric Pressure," *Journal of Applied Physics*, Vol. 108, No. 10, 2010, Paper 103306. doi:10.1063/1.3514131

[8] Moreau, E., and Touchard, G., "Enhancing the Mechanical Efficiency of Electric Wind in Corona Discharges," *Journal of Electrostatics*, Vol. 66, Nos. 1–2, 2008, pp. 39–44. doi:10.1016/j.elstat.2007.08.006

[9] Kim, C., Park, D., Noh, K., and Hwang, J., "Velocity and Energy Conversion Efficiency Characteristics of Ionic Wind Generator in a Multistage Configuration," *Journal of Electrostatics*, Vol. 68, No. 1, 2010, pp. 36–41. doi:10.1016/j.elstat.2009.09.001

[10] Bondar, H., and Bastien, F., "Effect of Neutral Fluid Velocity on Direct Conversion from Electrical to Fluid Kinetic Energy in an Electro-Fluid-Dynamics (EFD) Device," *Journal of Physics D: Applied Physics*, Vol. 19, No. 9, 1986, pp. 1657–1663. doi:10.1088/0022-3727/19/9/011

[11] Singhal, V., and Garimella, S. V., "Influence of Bulk Fluid Velocity on the Efficiency of Electrohydrodynamic Pumping," *Journal of Fluids Engineering Transactions of the ASME*, Vol. 127, No. 3, 2005, p. 484. doi:10.1115/1.1899173

[12] Go, D. B., Maturana, R. A., Fisher, T. S., and Garimella, S. V., "Enhancement of External Forced Convection by Ionic Wind," *International Journal of Heat and Mass Transfer*, Vol. 51, Nos. 25–26, 2008, pp. 6047–6053. doi:10.1016/j.ijheatmasstransfer.2008.05.012

[13] Ganan-Calvo, A., Davila, J., and Barrero, A., "Current and Droplet Size in the Electrospraying of Liquids. Scaling Laws," *Journal of Aerosol Science*, Vol. 28, No. 2, 1997, pp. 249–275. doi:10.1016/S0021-8502(96)00433-8

[14] Moreau, E., "Airflow Control by Non-Thermal Plasma Actuators," *Journal of Physics D: Applied Physics*, Vol. 40, No. 3, 2007, pp. 605–636. doi:10.1088/0022-3727/40/3/S01

[15] Benard, N., and Moreau, E., "Electrical and Mechanical Characteristics of Surface AC Dielectric Barrier Discharge Plasma Actuators Applied to Airflow Control," *Experiments in Fluids*, Vol. 55, No. 11, 2014, Paper 1846. doi:10.1007/s00348-014-1846-x

[16] Benard, N., Debien, A., and Moreau, E., "Time-Dependent Volume Force Produced by a Non-Thermal Plasma Actuator from Experimental Velocity Field," *Journal of Physics D: Applied Physics*, Vol. 46, No. 24, 2013, Paper 245201. doi:10.1088/0022-3727/46/24/245201

[17] Unfer, T., and Boeuf, J., "Modelling of a Nanosecond Surface Discharge Actuator," *Journal of Physics D: Applied Physics*, Vol. 42, No. 19, 2009, Paper 194017. doi:10.1088/0022-3727/42/19/194017

[18] Hagelaar, G. J. M., and Pitchford, L. C., "Solving the Boltzmann Equation to Obtain Electron Transport Coefficients and Rate Coefficients for Fluid Models," *Plasma Sources Science and Technology*, Vol. 14, No. 4, 2005, pp. 722–733. doi:10.1088/0963-0252/14/4/011

[19] Brown, T. T., "A Method of an Apparatus or Machine for Producing Force and Motion," G.B. Patent 300311, 1928.

[20] Brown, T. T., "Electrokinetic Apparatus," U.S. Patent 2,949,550, Aug. 1960.

[21] Christenson, E., and Moller, P., "Ion-Neutral Propulsion in Atmospheric Media," *AIAA Journal*, Vol. 5, No. 10, 1967, pp. 1768–1773. doi:10.2514/3.4302

[22] Wilson, J., Perkins, H., and Thompson, W., "An Investigation of Ionic Wind Propulsion," NASA TM-2009-215822, 2009.

[23] Pekker, L., and Young, M., "A Model of an Ideal Electrohydrodynamic Thruster," *Journal of Propulsion and Power*, Vol. 27, No. 4, 2011, pp. 786–792. doi:10.2514/1.B34097

[24] Masuyama, K., and Barrett, S. R. H., "On the Performance of Electrohydrodynamic Propulsion," *Proceedings of the Royal Society A*, Vol. 50, No. 6, 2013, pp. 1480–1486.

[25] Kiousis, K. N., Moronis, A. X., and Fruh, W. G., "Electro-Hydrodynamic (EHD) Thrust Analysis in Wire–Cylinder Electrode Arrangement," *Plasma Science and Technology*, Vol. 16, No. 4, 2014, pp. 363–369. doi:10.1088/1009-0630/16/4/11

[26] Moreau, E., Benard, N., Alicalapa, F., and Douyère, A., "Electrohydrodynamic Force Produced by a Corona Discharge Between a Wire Active Electrode and Several Cylinder Electrodes. Application to Electric Propulsion," *Journal of Electrostatics*, Vol. 76, May 2015, pp. 194–200. doi:10.1016/j.elstat.2015.05.025

[27] Gilmore, C. K., and Barrett, S. R. H., "Electrohydrodynamic Thrust Density Using Positive Corona-Induced Ionic Winds for In-Atmosphere Propulsion," *Proceedings of the Royal Society A*, Vol. 471, No. 2175,

2015, Paper 20140912.
doi:10.1098/rspa.2014.0912

[28] Grindley, G. C., "The Mobility of Ions in Air—Part 1. Negative Ions in Moist Air," *Proceedings of the Royal Society A*, Vol. 110, No. 754, 1925, pp. 341–358.

[29] Erikson, H. A., "On the Nature of the Negative and Positive Ions in Air, Oxygen and Nitrogen," *Physical Review*, Vol. 20, No. 2, 1922, pp. 117–126.
doi:10.1103/PhysRev.20.117

[30] Krylov, E. V., and Nazarov, E. G., "Electric Field Dependence of the Ion Mobility," *International Journal of Mass Spectrometry*, Vol. 285, No. 3, 2009, pp. 149–156.
doi:10.1016/j.ijms.2009.05.009

[31] Sigmond, R. S., "Simple Approximate Treatment of Unipolar Space-Charge-Dominated Coronas: The Warburg Law and the Saturation Current," *Journal of Applied Physics*, Vol. 53, No. 2, 1982, pp. 891–898.
doi:10.1063/1.330557

[32] Stuetzer, O. M., "Magnetohydrodynamics and Electrohydrodynamics," *Physics of Fluids*, Vol. 5, No. 5, 1962, pp. 534–544.
doi:10.1063/1.1706654

[33] Kim, C., Noh, K. C., Hyun, J., Lee, S. G., Hwang, J., and Hong, H., "Microscopic Energy Conversion Process in the Ion Drift Region of Electrohydrodynamic Flow," *Applied Physics Letters*, Vol. 100, No. 24, 2012, Paper 243906.

[34] Townsend, J. S., *Electricity in Gases*, Oxford Univ. Press, 1915, pp. 370–380.

[35] Roth, J., *Industrial Plasma Engineering, Principles*, Vol. 1, Inst. of Physics, London, 1995, pp. 256–275.

[36] Li, S., and Uhm, H., "Investigation of Electrical Breakdown Characteristics in the Electrodes of Cylindrical Geometry," *Physics of Plasmas*, Vol. 11, No. 6, 2004, pp. 3088–3095.
doi:10.1063/1.1736656

[37] Ponta, F. L., and Aref, H., "Strouhal-Reynolds Number Relationship for Vortex Streets," *Physical Review Letters*, Vol. 93, No. 8, 2004, pp. 1–4.
doi:10.1103/PhysRevLett.93.084501

[38] Stearns, R. G., "Ion Mobility Measurements in a Positive Corona Discharge," *Journal of Applied Physics*, Vol. 67, No. 6, 1990, pp. 2789–2799.
doi:10.1063/1.345445

J. Poggie
*Associate Editor*